Journal of Molecular Biology and Molecular Imaging

Open Access

Austin Publishing Group

Special Article - Cancer Imaging

Bioluminescent Imaging of Animal Models for Human Colorectal Cancer Tumor Growth and Metastatic Dissemination to Clinically Significant Sites

Fernández Y[1,2,6]*, Foradada L[1,2,6], García-Aranda N[1,2,6], Mancilla S[1,2,6], Suárez-López L[2,6], Céspedes MV[3,6], Herance JR[4,2], Arango D[5,6], Mangues R[3,6], Schwartz S Jr[2,6] and Abasolo I[1,2,6]*

[1]Functional Validation & Preclinical Research (FVPR), CIBBIM-Nanomedicine, Hospital Universitari Vall d'Hebron (HUVH) - Vall d'Hebron Institut de Recerca (VHIR), Universitat Autònoma de Barcelona (UAB), Barcelona, Spain

[2]Drug Delivery & Targeting, CIBBIM-Nanomedicine, HUVH-VHIR, UAB, Barcelona, Spain

[3]Grup d'Oncogènesi i Antitumorals of the Institut de Recerca de l'Hospital de la Santa Creu i Sant Pau, Barcelona, Spain

[4]Institut d'Alta Tecnologia-PRBB, Barcelona, Spain

[5]Molecular Oncology, CIBBIM-Nanomedicine, HUVH-VHIR, UAB, Barcelona, Spain

[6]Networking Research Center on Bioengineering, Biomaterials and Nanomedicine (CIBER-BBN), Barcelona, Spain

***Corresponding authors:** Fernández Y, Functional Validation & Preclinical Research (FVPR), CIBBIM-Nanomedicine, Hospital Universitari Vall d'Hebron (HUVH) - Vall d'Hebron Institut de Recerca (VHIR), Edifici Collserola – Lab 202; Passeig Vall d'Hebron, Spain, Tel: (+34) 934893000 ext. 3375; Fax: (+34) 932746708; Email: yolanda.fernandez.amurgo@vhir.org

Abasolo I, Functional Validation & Preclinical Research (FVPR), CIBBIM-Nanomedicine, Hospital Universitari Vall d'Hebron (HUVH) - Vall d'Hebron Institut de Recerca (VHIR), Edifici Collserola – Lab 202; Passeig Vall d'Hebron, 119-129; Spain

Received: May 07, 2015; **Accepted:** June 19, 2015; **Published:** June 22, 2015

Abstract

Purpose: Development of clinically-relevant mouse models which mimic natural tumor progression and metastatic dissemination of human colorectal cancer (CRC) is an essential requirement to better understand the mechanisms of cancer metastasis and to improve clinical therapeutics. A new era of modeling cancer metastasis involves the use of imaging technologies to monitor tumor growth and colonization after inoculation of cancer cells into the animals. This study reports on new experimental mouse models which mimics human CRC disease using noninvasive bioluminescent imaging (BLI).

Procedures: Luciferase-expressing HT-29 and HCT 116 cells were injected subcutaneously, orthotopically into the cecal wall, intrasplenically and intracardiacly into the left ventricle of nude mice. Tumor growth and metastatic dissemination patterns were monitored and quantified via *in vivo* and *ex vivo* BLI, and compared to tumor volume or histopathology. BLI results were validated using positron emission tomography (PET).

Results: Subcutaneous model validated BLI as a powerful tool for noninvasive monitoring and quantification of tumor growth and treatment efficacy, and for identifying new metastatic *foci*. Orthotopic colon model resembled the clinical pattern of CRC metastases that includes lymphatic, hematologic and coelomic dissemination. Furthermore, the intrasplenic and intracardiac models resulted in hepatic and bone-marrow metastases, respectively, sites with high clinical relevance in CRC. Importantly, in all models, BLI allowed the longitudinal follow-up of the CRC metastatic disease as it happens.

Conclusions: We provide improved and biologically relevant CRC experimental mouse models monitorable by BLI. These models are a valuable aid for the investigation on molecular mechanisms driving metastatic human CRC as well as on novel therapeutic strategies.

Keywords: Bioluminescent imaging; Positron emission tomography; Subcutaneous; Intracecal; Intrasplenic and intracardiac mouse models; Metastasis; Colorectal cancer

Abbreviations

BLI: Bioluminescent Imaging; CRC: Colorectal Cancer; FDG: 2-deoxy-2-[^{18}F]fluoro-D-glucose; Fluc: Firefly Luciferase; Fluc2: Firefly Luciferase 2; IC: Intracardiac; PET: Positron Emission Tomography; ph/s: Photons/second; SC: Subcutaneously; SEM: Standard Error of the Mean; SOI: Surgical Orthotopic Implantations

Introduction

Colorectal cancer (CRC) is one of the leading causes of cancer deaths in the western world. Metastatic dissemination of primary tumors is directly related to patient's survival and accounts for about 90% of all colon cancer deaths [1, 2]. Hence, the main problem in the treatment of CRC is not so much eradication of the primary tumor, but rather the formation of incurable metastases. The most common sites of metastasis in CRC patients are lymph nodes (55%), liver (45%) and lungs (22.5%) [3, 4]. Moreover, bone metastasis have previously been uncommonly reported [5], but its incidence has increased significantly in patients that have received multiple systemic treatments [6]. When such an event occurs, it is usually a late manifestation of the disease.

The biological processes that drive metastatic progression involve the success of cells in tissue invasion, intravasation, survival in the blood-stream and lymph, extravasation, and growth within a secondary organ [7]. It is therefore important to study tumor development and possible metastasis in biologically relevant environments, like the tissue from which they were derived or the tissue to which they metastasize. Thus, proper modeling of the early phases of spontaneous colorectal metastasis formation requires

Citation: Fernández Y, Foradada L, García-Aranda N, Mancilla S, Suárez-López L, Céspedes MV, et al. Bioluminescent Imaging of Animal Models for Human Colorectal Cancer Tumor Growth and Metastatic Dissemination to Clinically Significant Sites. J Mol Biol & Mol Imaging. 2015;2(2): 1019.

growing a metastatic tumor orthotopically in the intestine (e.g. cecum or rectum) [8]. Alternatively, in experimental metastasis models, early stages, including local invasion at the site of the primary tumor and gaining access to lymphatic or blood vessels, are bypassed by injection of tumor cells directly into systemic circulation. The site of injection in some cases defines which metastases will be developed. Thus, lateral tail-vein injection tends to mainly cause pulmonary metastases, whereas injection into the portal vein or spleen will usually elicit liver metastases [9], and intracardiac (i.c.) injection into the left ventricle of the heart introduces tumor cells to the arterial circulation leading to the colonization of cells to specific sites of the skeleton [10].

Traditionally, the follow-up over time of tumor burden and metastases development in orthotopic and experimental metastasis mouse models is limited to a specific endpoint which precludes longitudinal studies of metastases development *in vivo*. Observation of tumor growth kinetics as well as the determination of endpoints is therefore complex. The course of tumor development in time is then assessed by comparing groups of animals that were euthanized at different time points. Because of substantial inter-individual variation, large numbers of animals and laborious efforts are required, rendering the use of orthotopic and experimental metastasis models highly impracticable [11]. Nevertheless, access to technologies able to noninvasively detect molecular and biological processes in small animals such as bioluminescent optical imaging offer a new approach to overcome these drawbacks [12, 13]. Bioluminescent imaging (BLI) refers to light produced by an enzymatic reaction, usually between *Photinus pyralis* firefly luciferase (Fluc) enzyme and its substrate D-luciferin, in a reaction that requires oxygen and ATP [14]. The BLI backgrounds are extremely low, due to the fact that rodents do not naturally produce light, resulting in an excellent signal-to-noise ratio, and representing an extremely sensitive mean of detecting labeled cells [15]. Moreover, bioluminescence technology is fast and easy to perform, done in high-throughput, relatively inexpensive and suited for small animals compared to other preclinical functional imaging modalities available such as positron emission tomography (PET), which is radioactive and require a high degree of operational expertise, can be labor-intensive and is often cost prohibitive [16].

The elucidation of the molecular mechanisms of tumorigenesis and the development of therapeutic strategies to treat metastasized colorectal carcinoma require biologically relevant and adequate animal models in which tumor and metastasis progression of cancer cells are generated under well-controlled conditions. Thus, the aim of this study was to develop and provide to the scientific community more relevant animal models that are suitable to study CRC disease. In this study, the application of BLI to track and quantify tumor growth and therapeutic efficacy was first validated using subcutaneous mouse models, and then extended to orthotopic and experimental models. Orthotopic models were employed to reproduce the physiological colon environment and its spontaneous metastasis patterns, whereas experimental intrasplenic and intracardiac models were used to study colorectal liver and bone metastases, respectively.

Materials and Methods

Cells

Human CRC cell line HT-29 and HCT 116 were obtained from the ATCC (Rockville, MD, USA), and cultured in RPMI 1640 medium supplemented with 10% heat-inactivated fetal bovine serum (Lonza, Verviers, Belgium) and antibiotic-antimycotic (Invitrogen, Carlsbad, CA, USA) at 37ºC in a humidified atmosphere containing 5% CO_2.

Firefly luciferase and *firefly luciferase* 2 genes were cloned into the pcDNA3.1 vector (Invitrogen) and pGL4 (Promega Biotech Ibérica, Madrid, Spain), respectively. Cells were transfected using Lipofectamine 2000 (Invitrogen) and selected with 500 µg/mL of geneticin (Invitrogen). The HT-29.Fluc-C4 and HCT 116.Fluc2-C9 cell variants with the highest bioluminescent light emission were selected (Supplementary Information 1). These cell variants did not show changes in either growth rate or morphology in comparison with the parental cells (data not shown). Regarding to the luciferase expression of Fluc or Fluc2, in our hands, both luciferase genes worked similarly.

Bioluminescent imaging

BLI was performed using an IVIS® Spectrum imaging system (PerkinElmer, MA, USA) and the Living Image® 4.3 software (PerkinElmer) at the Molecular Imaging Platform of Vall d'Hebron Research Institute (VHIR) (Barcelona, Spain). For *in vivo* BLI, animals were given 150 mg/kg of D-luciferin (Promega) by intraperitoneal injection, and anesthetized using 1-3% isofluorane (Abbott Laboratories, IL, and USA). The light emitted from the bioluminescent cells was detected, digitalized and electronically displayed as a pseudocolor overlay onto a gray scale animal image. Regions of interest (ROI) from displayed images were drawn automatically around the bioluminescent signals and quantified as photons/second (ph/s). For *ex vivo* BLI, organs were removed 5-10 min after D-luciferin administration, incubated in 300 µg/mL D-luciferin solution, and imaged. All techniques were performed following procedures previously described in the literature [17-21].

Mouse models

Female athymic nude mice (Harlan Interfauna Iberica, Barcelona, Spain) were kept in pathogen-free conditions and used at 5-12 weeks of age. Animal care was handled in accordance with the Guide for the Care and Use of Laboratory Animals of the Vall Hebron University Hospital Animal Facility, and the experimental procedures were approved by the Animal Experimentation Ethical Committee at the institution. All *in vivo* experiments were performed at the CIBER-BBN's *In Vivo* Experimental Platform of the Functional Validation & Preclinical Research (FVPR) area (Barcelona, Spain).

Subcutaneous: HT-29.Fluc-C4 or HCT 116.Fluc2-C9 cells (1×10^6) were injected subcutaneously (s.c.) on the rear flanks of the mice (5-6 weeks, n=12-15). Tumor growth was monitored twice a week for 4-7 weeks by conventional caliper measurements ($D\times d^2/2$, where *D* is the major diameter and *d* the minor diameter) and *in vivo* BLI of the dorsal or lateral mouse views. Primary tumors were excised and secondary metastases were followed by *in vivo* BLI. At the end of the experiment, selected tissues were analyzed by *ex vivo* BLI and processed for histopathology.

For the efficacy studies, HT-29 tumor-bearing mice were randomized based on tumor volume (median, 125 mm^3) and tumor BLI (median, 4×10^8 ph/s) into 5-Fluorouracil (Sigma-Aldrich, Madrid, Spain) and PBS-control treatment groups (n=10/group).

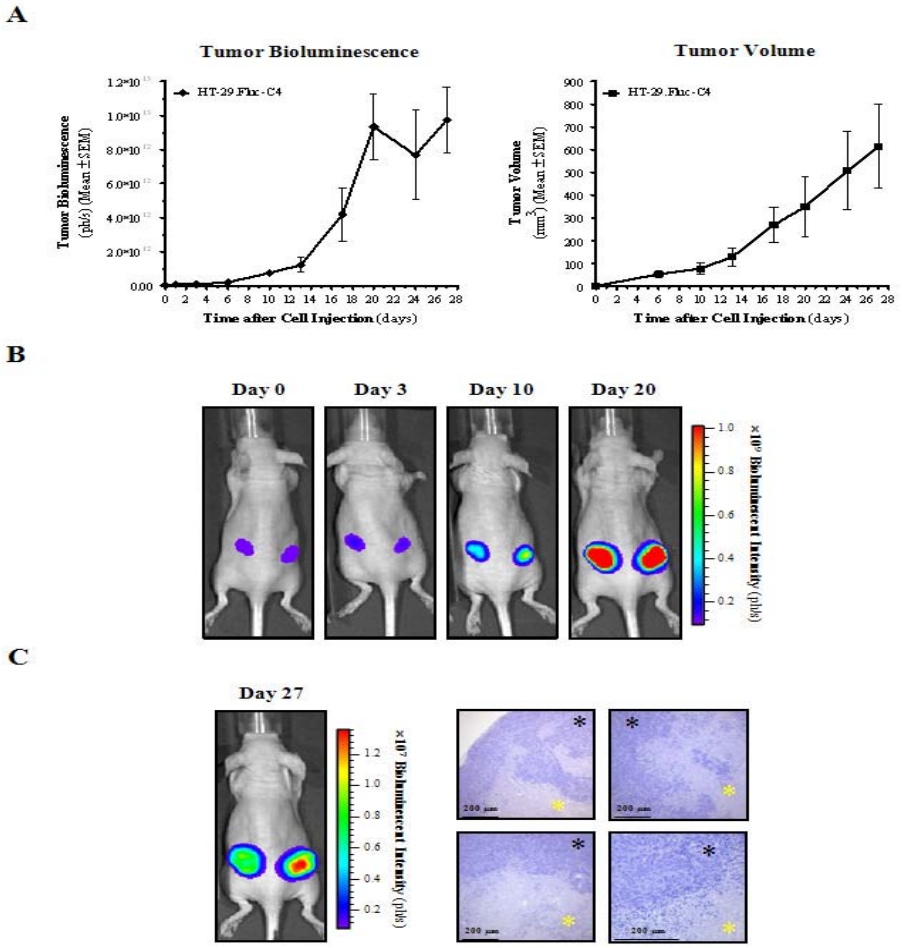

Figure 1: BLI to monitor and quantify subcutaneous tumor growth noninvasively.
A) Measurements of *in vivo* subcutaneous tumor bioluminescence and tumor volume over time. The total photons *per* second (ph/s) of the tumor region, and external measurements of tumor volume were quantified at each corresponding time point.
B) Data from one representative HT-29.Fluc-C4 subcutaneous bearing-tumor mouse is shown. Pseudocolor scale bars were consistent for all images from day 0 to 20 in order to show relative changes along time.
C) *In vivo* image of a representative HT-29.Fluc-C4 subcutaneous bearing-tumor mouse at day 27, and the corresponding histopathology of the excised tumor. *Black asterisks* indicate tumor cells, and *yellow asterisks* indicate necrotic tissue.

The 5-Fluorouracil was given at 50 mg/kg twice a week for 4 weeks by intravenous administration.

Orthotopic intracecum: The cecum of anesthetized mice (5-6 weeks, n=6-21) was exteriorized through a laparotomy, and 5×10^5 HT-29.Fluc-C4 or 2×10^6 HCT 116.Fluc2-C9 cells were injected under binocular lens into the cecal wall between the mucosa and the *muscularis externa* layers using a specially designed micropipette [22] or a 30-gauge needle attached to an insulin syringe. A proper implantation into the cecum was confirmed at day 0 by a localized and unique bioluminescent signal into the mice abdominal cavity. Mice successfully injected were imaged by BLI once a week from ventral and dorsal views. At termination, the gastrointestinal tract and the organs of interest were removed and examined by *ex vivo* BLI prior to the histological analyses. Moreover, two animals were imaged by PET (see section below).

Intrasplenic: To induce colorectal liver metastases the spleen of anesthetized mice (8-10 weeks, n=8-10) was exposed through a small left subcostal incision through the peritoneal wall, and 5×10^5 HT-29.Fluc-C4 or 1×10^6 HCT 116.Fluc2-C9 cells were injected into the spleen parenchyma. After 10 min, the splenic hilum was ligated and the spleen was removed to avoid intrasplenic tumor growth. The incision was closed and mice imaged to identify those with a successful intrasplenic injection, which were identified by a localized bioluminescent signal in the anatomic position of the liver. Metastatic growth was monitored once a week from ventral and dorsal views. Upon necropsy, liver, and other organs of interest were removed and examined by *ex vivo* BLI prior to histopathology.

Intracardiac: Anesthetized mice (10-12 weeks, n=8) were injected with 3×10^6 HT-29.Fluc-C4 cells into the left ventricle of the heart by nonsurgical means. Mice were then imaged to identify those with a successful i.c. injection, which was detected by an immediate but transient systemic bioluminescent signal over the entire animal. Only mice with evidence of a proper injection were included. The development of metastases was monitored once a week from ventral and dorsal views until endpoint criteria were reached. Upon

necropsy, all organs were excised and prepared for *ex vivo* BLI and histopathology.

Positron emission tomography

For PET imaging, 2-deoxy-2-[^{18}F]fluoro-D-glucose (FDG) was prepared using an IBA 18/9 cyclotron and a routine FDG synthesis module. Animals were fasted for 2 h and isofluorane anesthetized immediately before the intravenous injection of 10 MBq FDG. Animals were maintained awaken throughout the FDG uptake time (40 min) and anesthetized again to acquired static images for 10 min within a microPET R4 scanner (Concorde Microsystems, Knoxville, TN, USA), using an energy window of 350-650 keV and a coincidence window of 6 ns. The resulting list-mode data was sorted into 3D sinograms and images reconstructed by an Ordered Subset Expectation Maximization – Maximum-a-posteriori (OSEM3D-MAP) algorithm (18 iterations, 12 subsets) into a 128x128x63 (0.85x0.85x1.21 mm) matrix. Imaging data was corrected for non-uniformity response of the microPET, dead time count losses, and physical decay to the time of injection; no attenuation, scatter, or partial-volume averaging correction was applied. The same imaging procedure was applied for imaging *ex vivo* tissues. Parametric images based on standardized uptake value (activity concentration (MBq/ml) × body mass (g) / injected dose (MBq)) were generated for coronal, sagittal and transverse sections. For projected images, coronal sections covering the whole animal were fused using Amide software (Medical Image Data Examiner).

Histopathology

To confirm the presence of neoplastic cells, soft tissues samples were preserved in 4% formaldehyde solution and processed for histological analysis. Bones were fixed and decalcified using Decalcifier I (Surgipath Europe Ltd., Peterborough, UK). All tissues were paraffin embedded, sectioned, and stained with hematoxylin and eosin.

Results and Discussion

For many years, metastatic spread in experimental *in vivo* models could not be directly observed during the course of the disease. Tumor cells were injected at one site and metastatic dissemination determined *post mortem*. Advances in noninvasive imaging technologies have shed new light on the metastatic process, enabling now to watch metastasis as it develops. In this study, we have demonstrated that *in vivo* bioluminescent optical imaging allows the direct observation of cancer cells spreading from their site of origin and arriving at secondary sites longitudinally, offering early reads of disease progression and a rapid, sensitive and less invasive monitoring of neoplastic growth and metastases *versus* traditional cancer models. Specifically, we have provided novel mouse models to study metastatic CRC disease using the bioluminescent HT-29 and HCT 116 human colorectal cell lines.

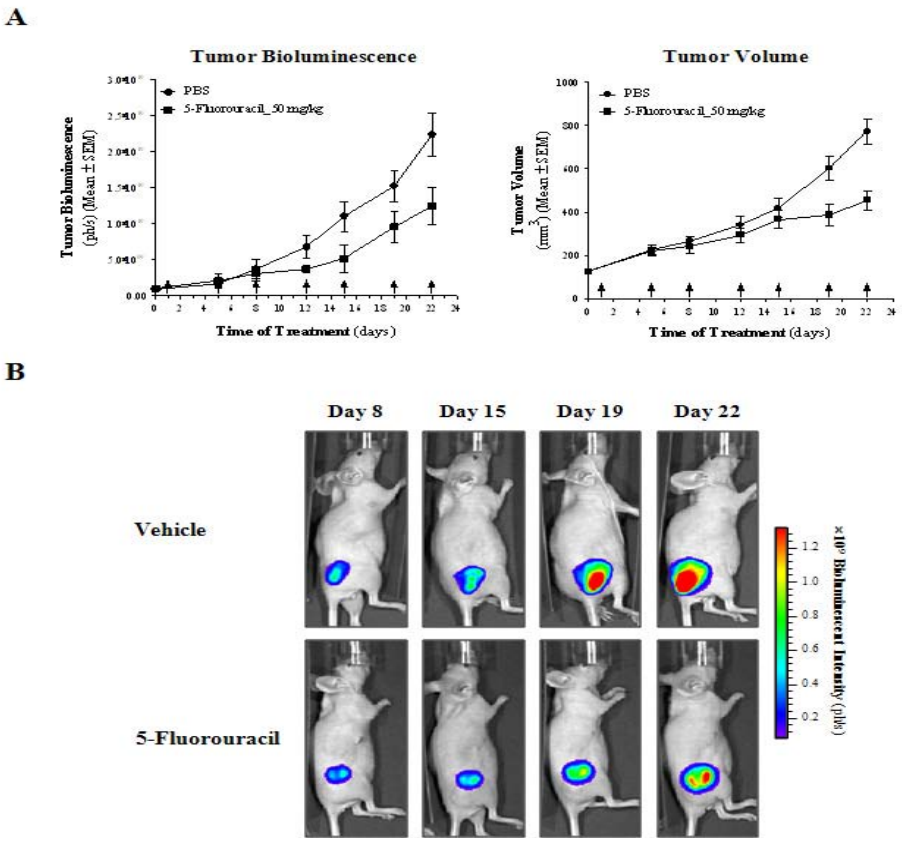

Figure 2: *In vivo* BLI monitoring of treatment efficacy of HT-29 subcutaneous tumors.
A) Measurements of *in vivo* subcutaneous tumor bioluminescence and tumor volume over time. *Arrows* indicate the time of treatment.
B) Lateral images of representative vehicle-control (PBS) and 5-Fluorouracil-treated mice are shown from day 8 to 22 after treatment. All images were set at the same pseudocolor scale to show relative bioluminescent changes over time.

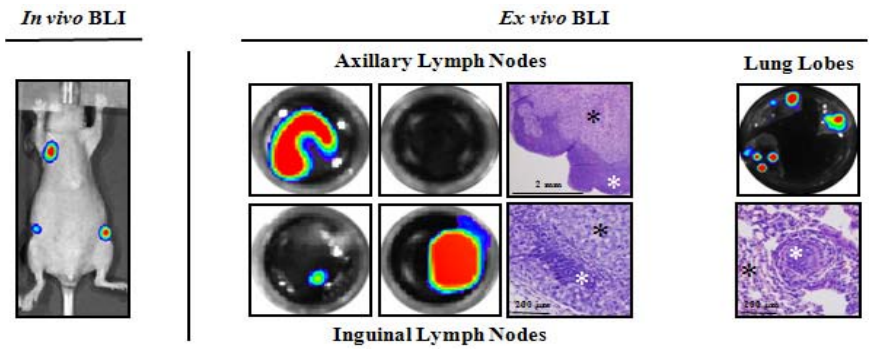

Figure 3: BLI to identify new metastatic sites of HT-29 subcutaneous tumors.
In vivo images of a representative mouse (*left panel*) show axillary and inguinal lymph node metastases development, and *ex vivo* BLI and histopathology of excised tissues (*right panel*) confirming the presence of lymphatic and hematogenous dissemination. *Black asterisks* indicate tumor cells, and *white asterisks* indicate normal tissue.

Bioluminescent imaging as a reliable tool to monitor and quantify tumor progression and treatment efficacy, and to identify new metastatic sites noninvasively

In order to validate the use of BLI for measuring tumor progression, HT-29.Fluc-C4 cells were implanted s.c. and tumor growth was monitored from the same day of inoculation by *in vivo* BLI and compared to external caliper measurements (Figure 1A, B). Bioluminescent signal at the injection site was visible on the inoculation day (day 0) while traditional caliper measurements could not begin until day 6. Tumor bioluminescence increased over time up to day 20, and a strong correlation between mean tumor bioluminescence and mean tumor volume was observed from day 6 to 20 (r^2=0.98, p=0.0015). These results indicate that the light emission from constitutively expressed Fluc is proportional to tumor cell burden, and changes of the bioluminescent signal over time accurately reflect tumor growth or regression. Moreover, the high sensitivity of BLI was effectively demonstrated in these subcutaneous tumor-bearing animals when tumors were immeasurable by means of a caliper, but quantification was feasible by photon emission calculation. Nonetheless, from day 20, tumor bioluminescence appears to plateau unlike the callipered tumor volume which continued to increase. Histopathological analyses of the HT-29 subcutaneous tumors further revealed that the bioluminescent plateau signal corresponds to tumors that have undergone central necrosis (Figure1C). Because bioluminescence is a function of the number of metabolically active tumor cells rather than a volumetric measure of the tumor mass, its ability to solely measure viable cells offers a great advantage and a more accurate value of tumor physiology over traditional volumetric-based measurements, which also include the contribution of dead or necrotic regions within a tumor.

In this context, we further demonstrated that BLI can be used to assess the efficacy of therapeutic interventions over time (Figure 2A, B). *In vivo* tumor bioluminescence and tumor volume showed tumor growth delay induced by 5-Fluorouracil (a pyrimidine analog, which it has been the established form of chemotherapy in the treatment of CRC for decades, that results in DNA damage and finally induces cell cycle arrest and apoptosis) when compared with vehicle control (p=0.0198 and p=0.0012, respectively, using a non-parametric Mann-Whitney U test). Statistically significant correlations were found between the mean tumor bioluminescence over time and the mean tumor volume of treated and control mice (r^2=0.89, p=0.0004 and r^2=0.98, p<0.0001, respectively). Thus far, our assessment confirms the ability of BLI to provide noninvasive, semi quantitative, and spatiotemporal information about tumor progression and response to therapy, as it has been shown for prostate [23], colon [19], brain [24], liver [25], and neuroblastoma [26] cancer, among others. Moreover, in drug evaluation, BLI can also serve as an accurate guide for timing the start or end of treatment in these therapeutic studies since one can immediately assess the tumor growth in each animal rather than depend upon data from animal cohorts euthanized at similar time points, thereby diminishing the dispersion introduced by interindividual variation in response to therapy and yielding to tremendous statistical benefit to the study [17, 27].

Spontaneous metastases from subcutaneous tumors are rare in animal models of cancer [28]. By means of *in vivo* BLI, as the whole animal was imaged, for the HT-29.Fluc-C4 model, we identified metastatic lesions growing into the axillary and inguinal lymph nodes regions (Figure 3). *Ex vivo* BLI and histopathology confirmed the presence of spontaneous metastases into lymph nodes and lungs (Figure 3 and Table 1) as Jenkins *et al.* [19] showed using SCID-beige mice. In fact, *in vivo* BLI is less suited for the identification of the exact location of tumors, because its spatial resolution is limited, by the attenuation due to the depth of the lesions and the cell number present in the bioluminescent sources. Spatial resolution can be obtained afterwards by macro- and microscopical inspection of relevant tissues through guidance with *ex vivo* BLI and histopathology. Thus, *ex vivo* BLI provides a very fast, reliable and sensitive method of screening for metastatic lesions, dictating which tissues should be further analyzed by histopathology to detect micro metastases, and

Table 1: Dissemination patterns from subcutaneous HT-29 and HCT 116 CRC bioluminescent cells.

	Spontaneous Metastasis Incidence [Mice (%)]	
	HT-29.Fluc-C4	**HCT 116.Fluc2-C9**
Lymphatic dissemination:		
Axillary lymph nodes	8/12 (67)	0/15 (0)
Inguinal lymph nodes	9/12 (75)	0/15 (0)
Hematologic dissemination:		
Lungs	7/12 (58)	0/15 (0)

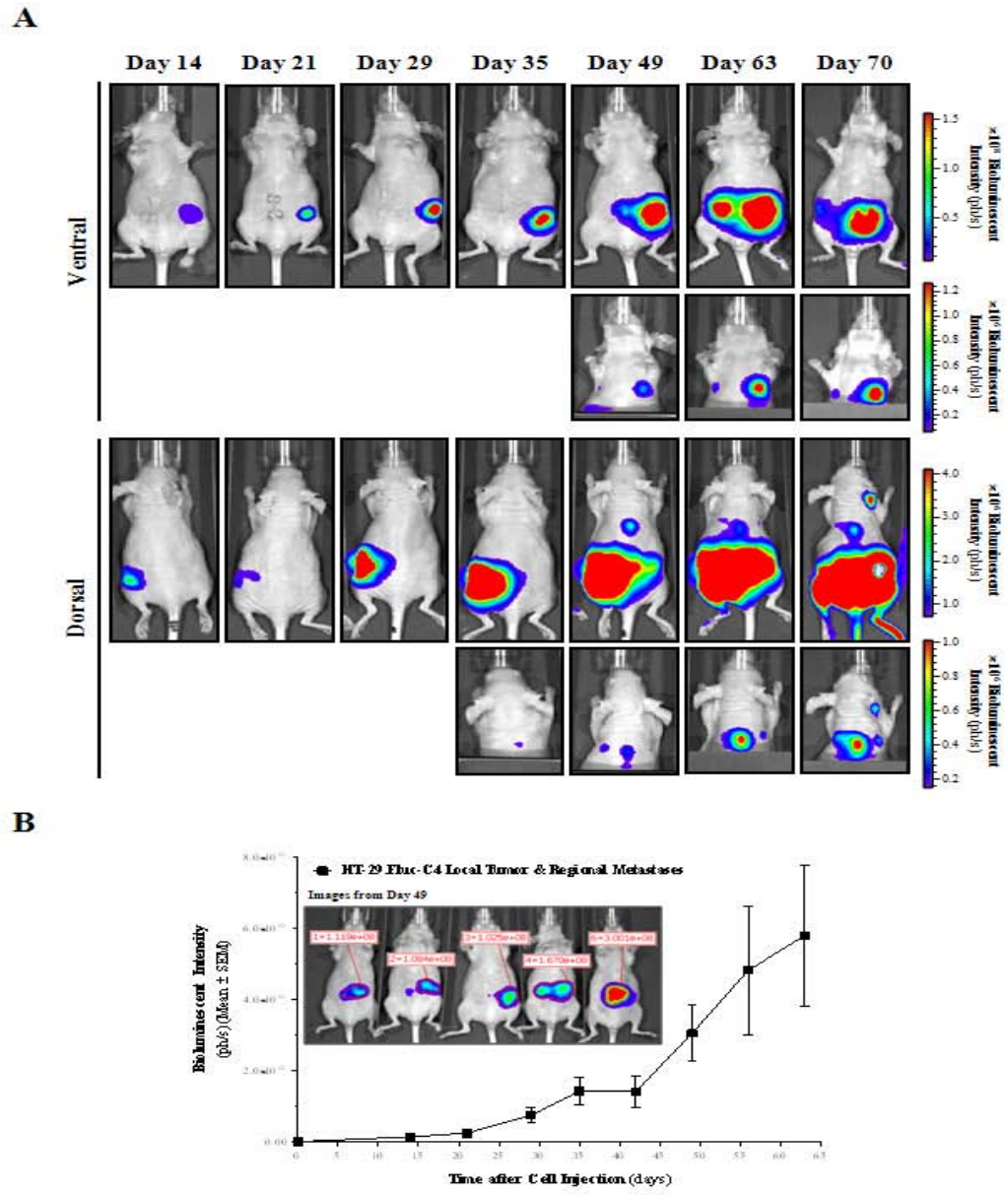

Figure 4: *In vivo* BLI of orthotopic HT-29 colorectal tumor progression and metastatic dissemination.
A) Selected ventral and dorsal view images from a representative mouse over time are shown. To check for metastasis development into the upper part of the mouse, animals were imaged with the primary tumor shielded. Images from each corresponding view were set at the same pseudocolor scale to show relative bioluminescent changes along time.
B) Primary tumors and regional metastases growth rate from the ventral abdominal region was quantified weekly by means of bioluminescent intensity (ph/s). A region of interest (ROI) for each animal (n=21) was defined at every time point (*inset*).

consequently reducing the number of histology rounds required. Moreover, metastases were not detected in any other tissues by BLI, as confirmed through a serial histopathological analysis. In contrast, for the HCT 116.Fluc2-C9 tumor model, no spontaneous metastases from subcutaneous tumors were detected into lymph nodes and lung tissues, among others (Table 1), which might be associated with a less aggressive and invasive HCT 116 cell phenotype compared to HT-29 cells. As a result, we further characterize and identify two subcutaneous CRC models with different dissemination patterns to study advanced CRC disease.

Improved orthotopic colorectal cancer mouse models to study noninvasively primary tumor growth and clinically-relevant metastases

The major limitations of subcutaneous CRC mouse models are that they do not recapitulate many of the essential features of tumor growth in patients, rarely metastasize, and the ectopic microenvironment greatly differs from that in the colon. Interactions between the host environment and the tumor graft determine tumor cell expression profiles, the levels of growth factors and nutrients, as well as tumor angiogenesis and metastatic behavior [29, 30]. In

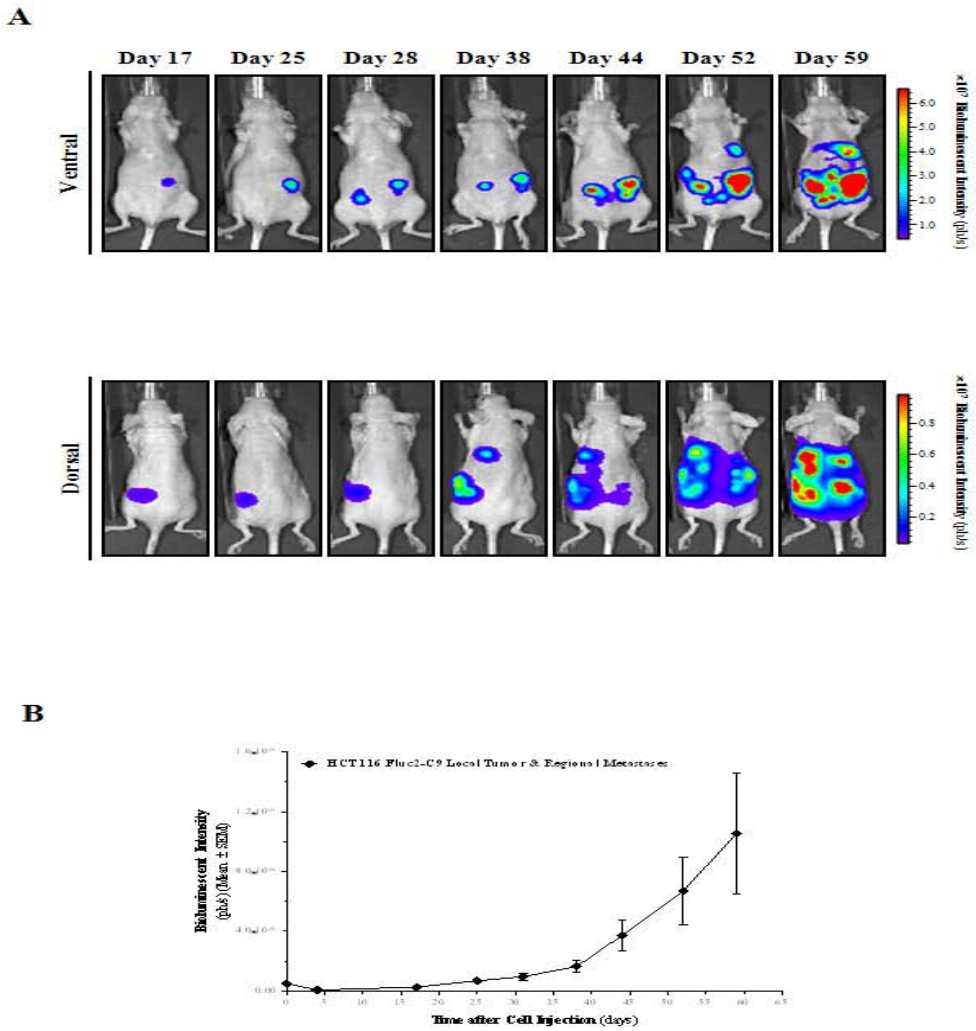

Figure 5: *In vivo* BLI of orthotopic HCT 116 colorectal tumor progression and metastatic dissemination.
A) Selected ventral and dorsal view images from a representative mouse over time are shown. Images from each corresponding view were set at the same pseudocolor scale to show relative bioluminescent changes along time.
B) Primary tumors and regional metastases growth rate from the ventral abdominal region was quantified weekly by means of bioluminescent intensity (ph/s).

addition, ectopic and orthotopic organ environments differentially influence the sensitivity of tumor cells to chemotherapeutics [31]. Likely, the most relevant application of imaging in preclinical models is the use of whole-body BLI to longitudinally track both primary and metastatic tumor burden in orthotopic and deep-tissue models, because in many cases they are neither visible nor palpable at the tissue surface. Previously, Céspedes *et al.* [22] have improved the orthotopic injection of human CRC cell lines by direct orthotopic cell microinjection, generating a model in which the dissemination pattern closely replicates all relevant metastatic sites observed in humans. Then, bioluminescent colorectal HT-29 and HCT 116 cells were directly injected into the cecal wall of mice, and tumor growth and metastatic dissemination monitored in real time by *in vivo* BLI. Inappropriately implanted mice were discarded at the inoculation day based on BLI determinations, something that could not have been done without BLI (Supporting Information 2A). *In vivo* BLI of orthotopic tumors identify bioluminescent lesions developing in the abdominal (primary tumor and locoregional dissemination) and thoracic (distant dissemination) cavities for HT-29.Fluc-C4 tumors (Figure 4A), and only in the abdominal cavity for HCT 116.Fluc2-C9 tumors (Figure 5A) as early as days 49 and 28 after implantation, respectively. Hence, HT-29.Fluc-C4 tumors induce a preferred distant metastasis dissemination pattern compared to HCT 116. Fluc2-C9 tumors which favored a more locoregional invasion pattern near the primary tumor site. Bioluminescent signals were quantified over time to determine the HT-29.Fluc-C4 (Figure 4B) and HCT 116.Fluc2-C9 (Figure 5B) orthotopic colon tumor growth into the abdominal cavity. A steady increase of bioluminescent signals, which corresponds with local colonic tumor and locoregional lymphatic dissemination of implanted colon tumor cells, was observed a long time.

When either intestinal obstructions (15 out of 21 (71%) for HT-29, and 0 out of 10 (0%) for HCT 116 tumors) or tumor growing towards the peritoneal cavity (6 out of 21 (29%) for HT-29, and 8 out of 9 (89%) for HCT 116 tumors) appeared, animals were euthanized and a complete necropsy procedure performed. The median survival

Table 2: Dissemination patterns from orthotopic HT-29 and HCT HCT 116 CRC bioluminescent cells.

	Spontaneous Metastasis Incidence [Mice (%)]	
	HT-29.Fluc-C4	**HCT 116.Fluc2-C9**
Lymphatic dissemination:		
Mesenteric lymph nodes	20/21 (95)	6/6 (100)
Peripancreatic lymph nodes	15/21 (71)	3/6 (50)
Inguinal lymph nodes	9/21 (43)	2/6 (33)
Axillary lymph nodes	6/21 (29)	1/6 (17)
Hematologic dissemination:		
Liver	17/21 (81)	0/6 (0)
Lungs	19/21 (90)	4/6 (67)
Coelomic dissemination:		
Diaphragm	6/21 (29)	5/6 (83)
Carcinomatosis	6/21 (29)	5/6 (83)

time of animals was 77 (ranged from 49 to 96) and 65 (ranged from 59 to 87) days for the HT-29.Fluc-C4 and HCT 116.Fluc2-C9 tumors, respectively. *Ex vivo* BLI and histopathological analyses of the isolated tissues confirmed the induction of lymphatic, coelomic and hematogenous dissemination patterns at different incidence rates based on the tumor model (Table 2). Besides lymphatic dissemination, hematological dissemination and coelomic invasion were the most preferred dissemination patterns on the HT-29.Fluc-C4 and HCT 116.Fluc2-C9 orthotopic tumors, respectively. Thus, in HT-29. Fluc-C4 (Figure 6) and HCT 116.Fluc2-C9 (Figure 7) tumor-bearing animals, local orthotopic tumor growth and mesenteric lymphatic tumor *foci* were detected. Further, tumor *foci* were also frequent in peripancreatic, inguinal and axillary lymphatics. Liver or lung metastases, the most common sites for blood-borne metastases in human CRC, were mainly detected on HT-29.Fluc-C4 tumors (Table 2). Finally, tumors growing towards the peritoneal cavity inducing peritoneal carcinomatosis and invasion of the mesenteric lymphatic, among other organs were the preferentially occurring on HCT 116. Fluc2-C9 orthotopic tumors. *Ex vivo* BLI negative organs such as spleen, kidneys, adrenal glands, brain and bones, were also found histologically negative for tumor cells.

As for the orthotopic colon tumor mouse models monitored noninvasively available in the literature, characterization of human CRC cells in a surgical orthotopic implantations (SOI) or cell implantation models using fluorescent proteins as tumor cell markers has been described and employed to further characterize novel colonoscopic imaging agents [32-34]. Related to the use of these fluorescent proteins as genetic reporters *in vivo*, green or red fluorescent proteins require an excitation at wavelengths that penetrate tissue layers with difficulty, and are limited by the presence of significant tissue auto fluorescence, which consequently decreases the sensitivity of this technique when compared to BLI [16]. In fact, HCT 116 and HT-29 CRC bioluminescent orthotopic cecal wall models in SCID and NSG mice, respectively, has been successfully used to evaluate the role of chemokines in the inhibition of orthotopic primary tumor and locoregional lymph node metastases formation [35], and the role of anti-metastatic effect of immune effectors in the inhibition of the primary tumor growth and the emerging secondary

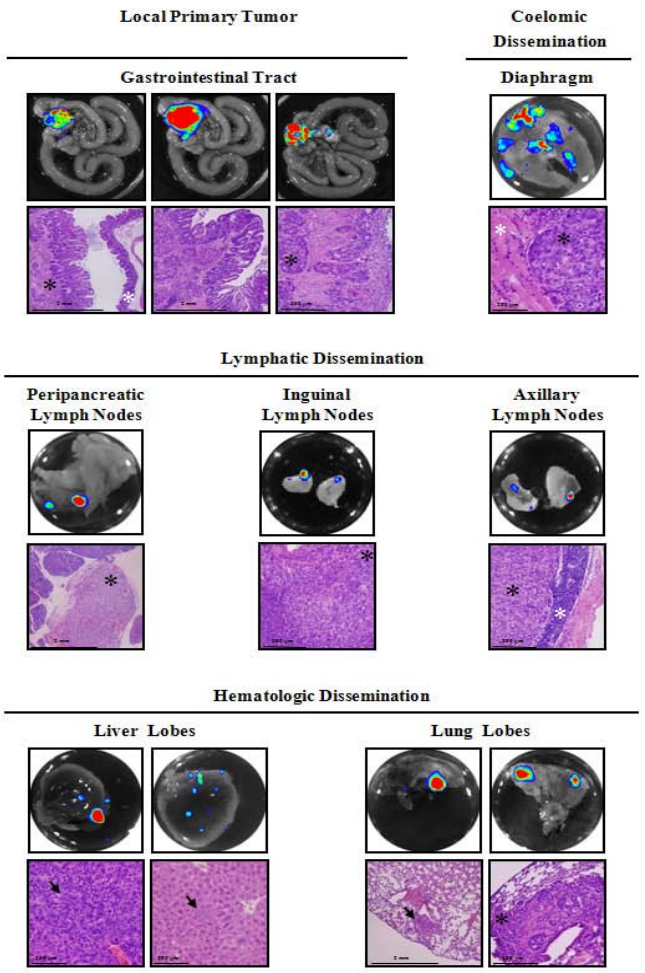

Figure 6: *Ex vivo* BLI and histological analysis from orthotopic HT-29 colorectal tumor-bearing mice.
Ex vivo images and histopathology of excised tissues from a representative mouse show local primary tumor growth (poorly differentiated adenocarcinoma, invading the submucosa, the hyperplastic mucosa and the cecal muscularis), and coelomic dissemination (tumoral cells infiltrating muscular tissue of the diaphragm), lymphatic dissemination (total effacement of a peripancreatic lymph node, tumor cells infiltrating an inguinal lymph node, and tumoral *foci* leaving a rim of normal axillary lymphoid tissue) and hematologic dissemination (liver parenchyma and sinusoids infiltrated by neoplastic cells with a mixed inflammatory reaction, and isolated micrometastasis in the interstitium of the lung and tumoral embolus occluding peribronchial blood vessels). *Black asterisks* or *arrows* indicate tumor cells, and *white asterisks* indicate normal tissue.

tumor *foci* in the lungs and liver [36]. Moreover, we previously demonstrated the ability to use BLI to validate antitumor and antimetastatic treatment strategies using a luciferase-expressing HT-29 CRC cells forming tumors in the cecum wall of nude mice and metastasizing to lymphatic, hematological and coelomic tissues [21]. In our case, bioluminescent HT-29 and HCT 116 orthotopic colon models resemble the clinical spreading patterns of CRC metastases reproducing lymphatic, hematologic and coelomic dissemination patterns, and favoring different outcomes depending on both the intrinsic metastatic capacity of the tumor cells and the influence of the implantation organ environment. These models drive tumor cells to infiltrate the lymphatics of the intestinal wall, disseminating

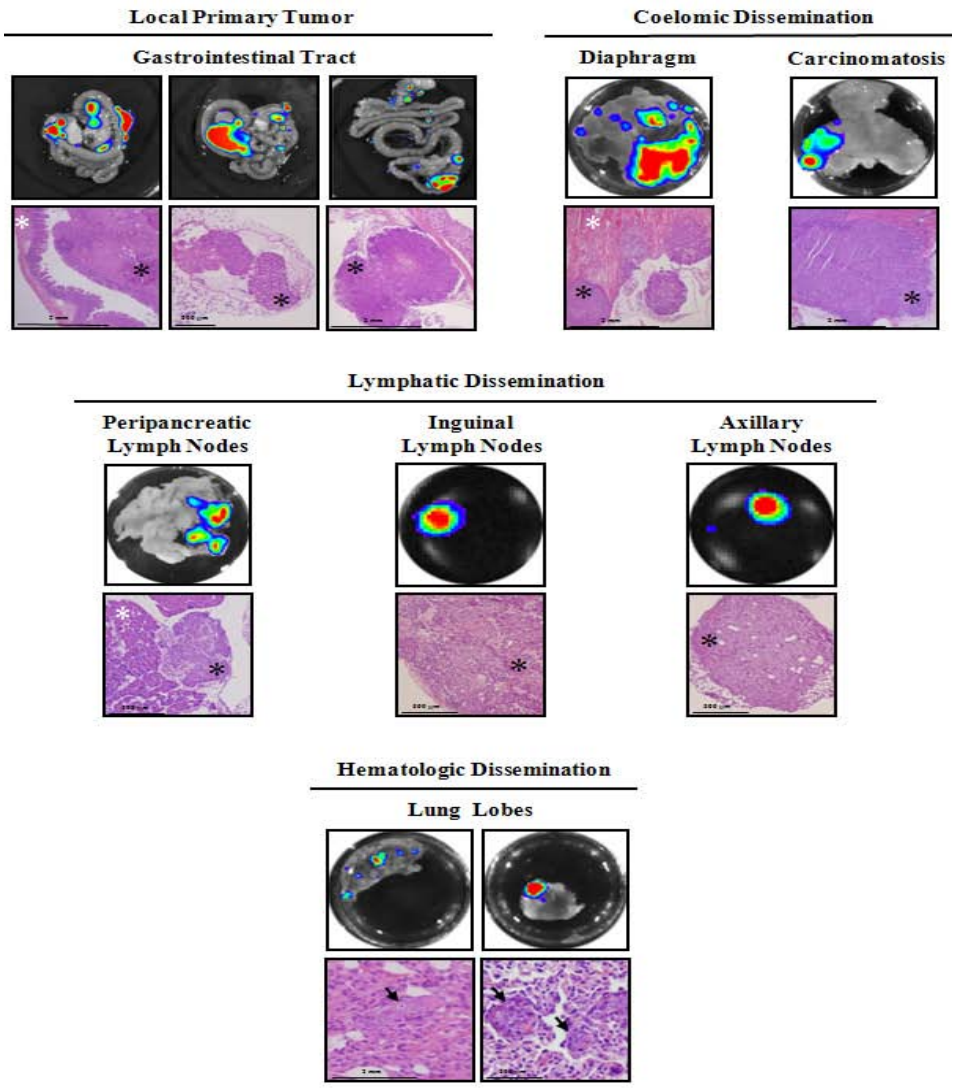

Figure 7: *Ex vivo* BLI and histological analysis from orthotopic HCT 116 colorectal tumor-bearing mice.
Ex vivo images and histopathology of excised tissues from a representative mouse show local primary tumor growth (poorly differentiated adenocarcinoma, invading one side of the cecal lamina and submucosas while the opposite one remains normal (*left picture*), metastatic embolus inside a mesenteric lymphatic vessel (*middle picture*) and tumoral invasion of a lymphatic from the glandular stomach wall (*right picture*), and coelomic dissemination (multiple carcinomatous *foci* infiltrating diaphragm muscular fibers and muscular layers of the abdominal wall from its peritoneal side), lymphatic dissemination (peripancreatic, inguinal and axillary lymph nodes invaded by metastatic cells) and hematologic dissemination (distant micrometastases in the lung parenchyma and inside blood vessels). *Black asterisks* or *arrows* indicate tumor cells, and *white asterisks* indicate normal tissue.

first into the mesenteric lymph nodes, and after spreading through the blood-stream into the liver and lung, and/or to the peritoneum, at significantly higher rates compared with SOI of tumor fragments [37]. Moreover, the orthotopic cell microinjection procedure does not produce significant tissue damage and avoids cell reflux, which eventually could mask carcinomatosis spread. Thus, we provided noninvasive bioluminescent orthotopic CRC mouse models with different metastatic dissemination patterns that replicate human disease with high fidelity, and therefore, the clinical setting. Accordingly, longitudinal studies allow the assessment of the course of tumor progression and metastases development in asymptomatic animals which contributes to generate more informative and predictive animal models of cancer and an attractive alternative to test the efficacy of treatments, in particular at early phases when therapeutical options should be most effective. Furthermore, as the whole animal is imaged, unpredictable sites of metastasis are evident and can be rapidly identified.

BLI also has limitations (low tissue penetration, low spatial resolution, requirement of an exogenous substrate, etc.) [38]. Therefore, in order to validate our model with imaging techniques routinely used in the clinics, few animals were also imaged by means of small animal devoted PET. This would further evaluate the potential of small animal BLI *versus* PET using FDG, the most commonly used radiotracer in the clinical practice (Figure 8A). Tumors have high rates of aerobic glycolysis, and therefore take up relatively large amounts of the glucose analogue FDG by glucose transporters [39, 40]. Bioluminescent signals indicate primary tumor growth

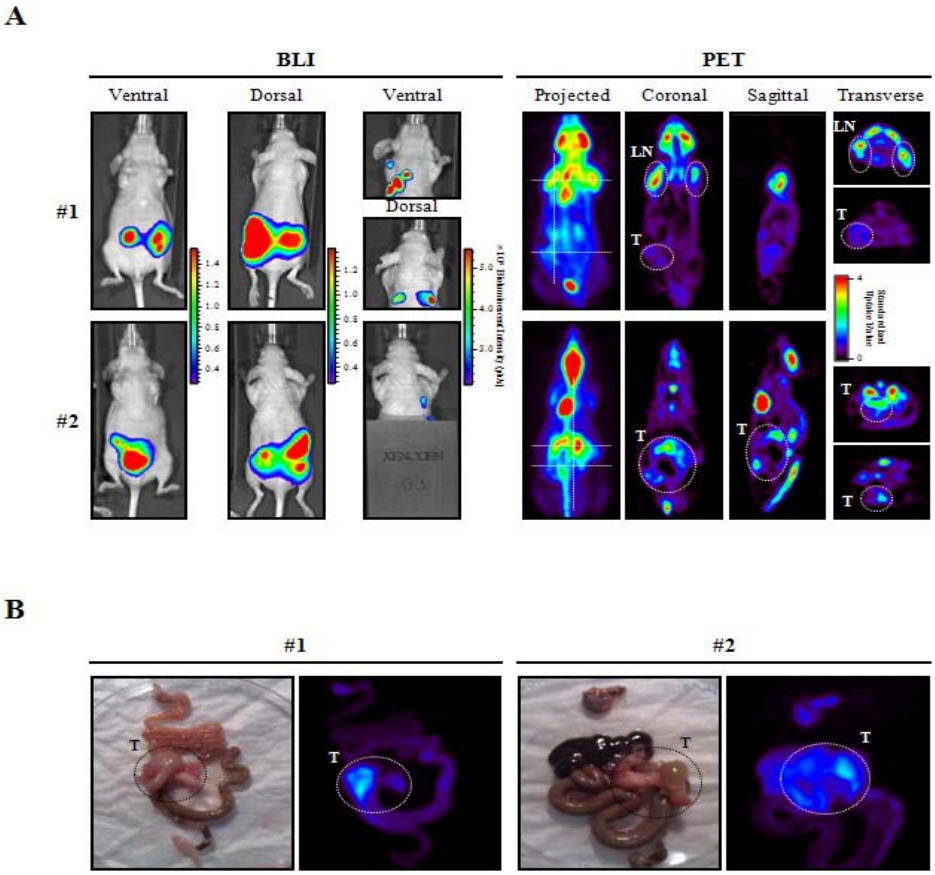

Figure 8: Comparison of BLI and PET *in vivo* imaging of HT-29 orthotopic CRC mouse model.
A) At day 87 after cell implantation, mice were imaged by BLI and one day after by PET using FDG as a tracer. For BLI (*left panel*), ventral and dorsal view images with and without the abdominal body region shield are shown, and for PET (*right panel*) projected images, coronal, sagittal, transverse thoracic and abdominal representative sections are also shown for each mouse. *Dotted lines* in the projected image indicate the localization of sagittal and transverse sections. Animal #1 shows a clear uptake in axillary lymph nodes (LN) and a lower signal in the primary tumor (T); and animal #2 has a higher uptake in the primary tumor, which extends considerably in the abdominal region. Heart and brain, and kidney and bladder showed high glucose uptake due to intrinsic high metabolic activity and FDG clearance, respectively.
B) *Ex vivo* PET analyses of excised tissues further confirmed the localization of *in vivo* signals. Localization of colorectal primary tumors is indicated.

and locoregional metastases growing in the abdominal cavities and disseminated lesions developing in the thoracic cavities. Even though PET could provide more accurate tomographic information than BLI, the high background uptake of FDG in heart, muscle, brown fat, kidney, bladder and brain interfered with the primary tumor and metastatic lesions detection. However, with greater difficulty than BLI, PET imaging detected the primary tumor growing within the abdominal cavity and metastatic lesions developing in axillary lymph nodes. *Ex vivo* PET of the gastrointestinal tract helped to identify the increased FDG uptake of the primary tumor (Figure 8B). Novel molecules with better imaging quality characteristics such as 3'-[^{18}F]fluoro-3'-deoxythymidine [41] or reporter specific tracers [42, 43] would increase the signal-to-noise ratio and might improve the detection of metastasis since they show higher absolute uptakes and lower gastrointestinal activities than FDG. Therefore, each technology represents a valuable tool to study tumor-bearing animals, but the careful selection of the most appropriate method will be critical to maximize the benefit of their use. Here, BLI provides a higher sensitivity compared to PET imaging when using FDG, and being a very convenient modality for the preclinical oncology research.

Novel noninvasive bioluminescent liver and bone metastasis models of colorectal cancer

The use of experimental metastasis models is an excellent option to study the late steps of metastasis formation such as extravasation, colonization and growth in secondary tissues. Importantly, due to its high sensitivity, BLI is very useful for early detection of micrometastases and minimal residual disease states in animal models [44-46] such as in the intrasplenic and intracardiac models that we have characterized to further study liver and bone metastasis. In general, orthotopic mouse models do not permit the study of the progression of hepatic and bone metastases because the life of the animals is compromised before they progress or appear. Thus, the capacity of HT-29.Fluc-C4 and HCT 116.Fluc2-C9 cells to produce metastatic growth in the liver was monitored by BLI subsequent to injection of cells into the spleen. Mice with no or very low bioluminescent signal were excluded from the study on the injection day (Supporting Information 2B). Bioluminescent lesions developing in the abdominal cavity localized with the anatomic position of the liver were identified for HT-29. Fluc-C4 (Figure 9A) and HCT 116.Fluc2-C9 tumors. A progressive growth increase of the hepatic bioluminescent signal was quantified

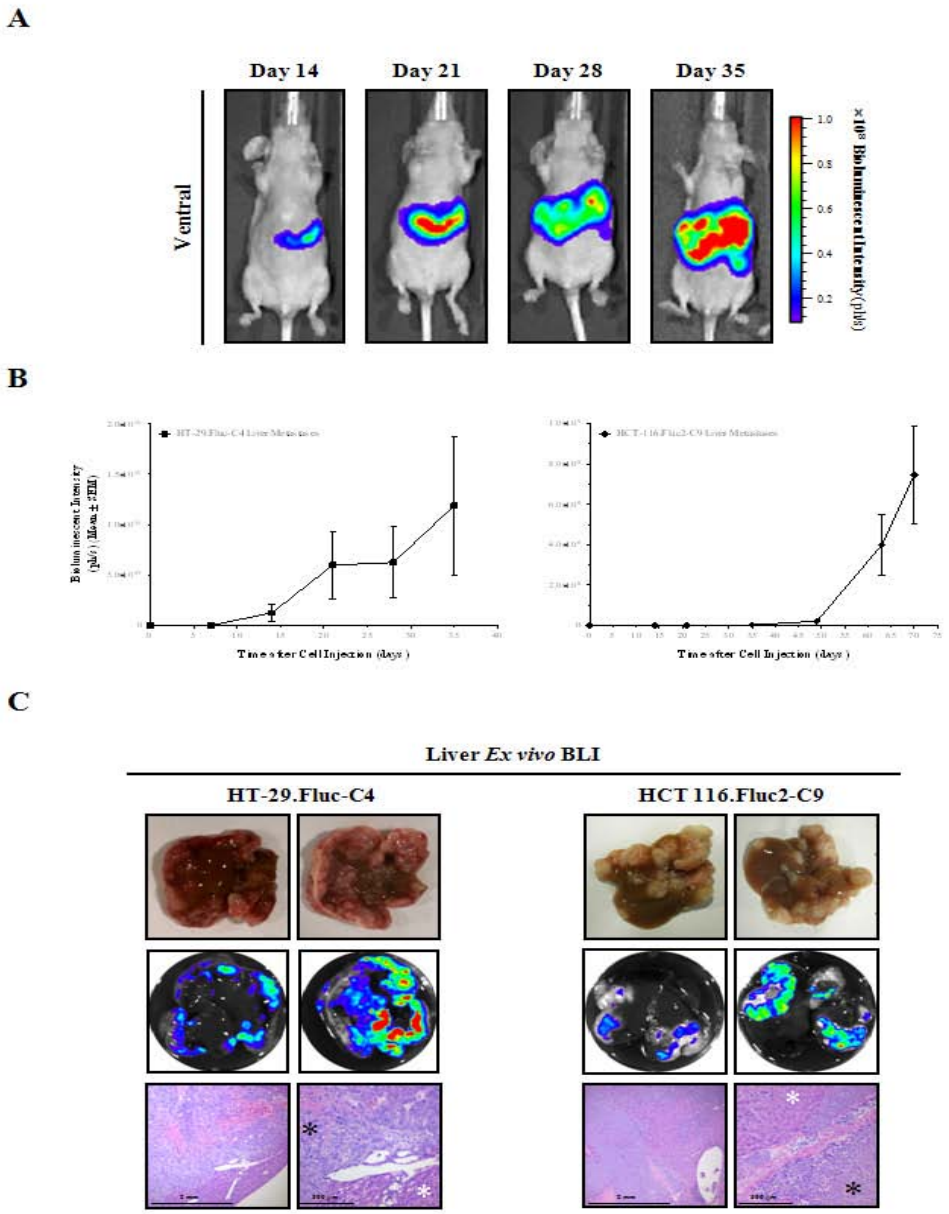

Figure 9: Hepatic metastases detected *in vivo* and *ex vivo* following intrasplenic injection of HT-29 and HCT 116 bioluminescent cells.
A) Ventral images taken longitudinally of a representative mouse are shown. Images were set at the same pseudocolor scale to show relative bioluminescent changes along time.
B) Bioluminescent metastatic growth rate was quantified along time in the liver region (ph/s).
C) Liver photographs, *ex vivo* BLI and histopathology confirmed the localization of *in vivo* BLI signals into liver parenchyma. Multiple neoplastic *foci* infiltrating the liver parenchyma mixed with mononuclear inflammatory, hemorrhagic and necrotic areas. *Black asterisks* indicate tumor cells, and *white asterisks* indicate normal tissue.

along time; inducing HT-29.Fluc-C4 tumors a faster growth than the HCT 116.Fluc2-C9 (Figure 9B). The median overall survival of animals was 61 (ranged from 35 to 85) and 83 (ranged from 81 to 83) days for the HT-29.Fluc-C4 and HCT 116.Fluc2-C9 tumors, respectively. *Ex vivo* BLI and histopathology of the isolated tissues confirmed the induction of the liver, lung and carcinomatoses metastases at different incidence rates based on the tumor cell model (Figure 9C and Table 3). As a result, we describe two mouse models of CRC liver metastases with different patterns of dissemination by BLI, providing longitudinal data on tumor growth *in vivo*, and

Table 3: Metastatic lesions after intrasplenic injection of HT-29 and HCT 116 CRC bioluminescet cells.

	Metastasis Incidence [Mice (%)]	
	HT-29.Fluc-C4	**HCT 116.Fluc2-C9**
Hematologic metastases:		
Liver	6/8 (75)	6/10 (60)
Lungs	6/6 (100)	6/6 (100)
Coelomic metastases:		
Carcinomatosis	0/6 (0)	4/6 (67)

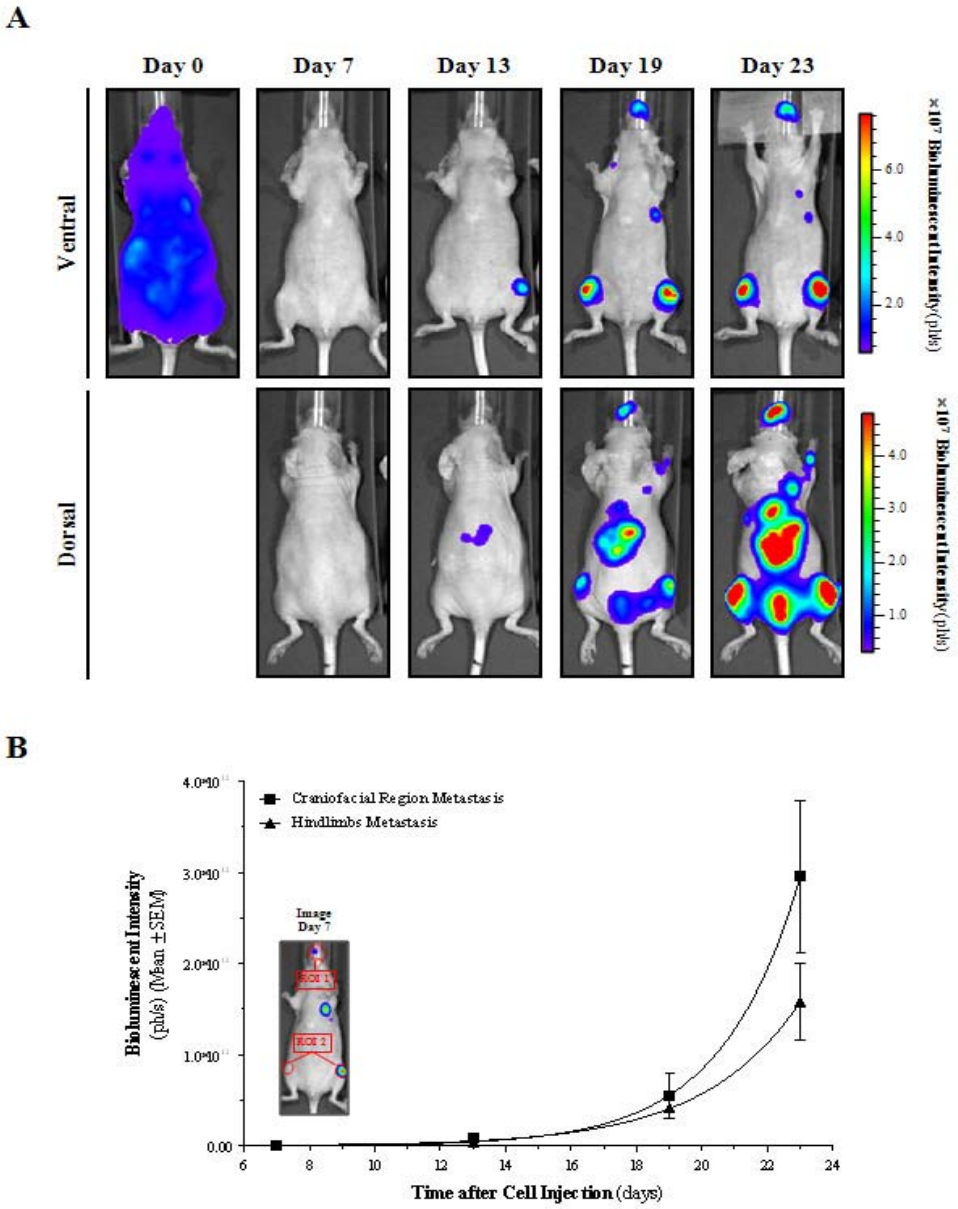

Figure 10: Multiple metastases detected *in vivo* following intracardiac injection of HT-29 bioluminescent cells.
A) Ventral and dorsal images taken longitudinally of a representative mouse are shown. Images from each corresponding view were set at the same pseudocolor scale to show relative bioluminescent changes along time.
B) Metastatic growth rate was quantified longitudinally in the craniofacial (ROI 1) and hindlimbs (ROI 2) regions.

offering a more accurate representation of the intrahepatic clinical disease. Accordingly, the use of BLI for measuring experimental CRC growth in the liver has already been proof as a reliable and superior method (simplicity, reduced laboriousness, possibility to randomize, possibility to perform consecutive measurements) for other CRC cells [20, 47].

To establish a model of bone metastases *in vivo*, the CRC HT-29. Fluc-C4 cells, which showed enhanced hematological dissemination patterns, were injected into the left ventricle of the heart to allow the dispersion of cells into the blood-stream without first passing through the lungs. The properly injected mice (Supporting Information 2C) were imaged *in vivo* along time (Figure 10A). Metastatic growth became evident as early as day 7 after cell injection, mimicking micrometastatic spread (Figure 10B, *inset*). Patterns of metastasis indicating lesions developing in the craniofacial, thoracic and abdominal regions and hindlimbs were observed (Figure 10A). None of these tumors were macroscopically visible. Quantification of the bioluminescence intensity of the craniofacial and hindlimbs lesions confirmed that the metastatic sites showed an exponential increase in bioluminescence over time (Figure 10B), indicating that bioluminescent measurements can be used to monitor the metastatic growth noninvasively along time. *Ex vivo* BLI confirmed that the metastatic spread of HT-29.Fluc-C4 colorectal cells after i.c.

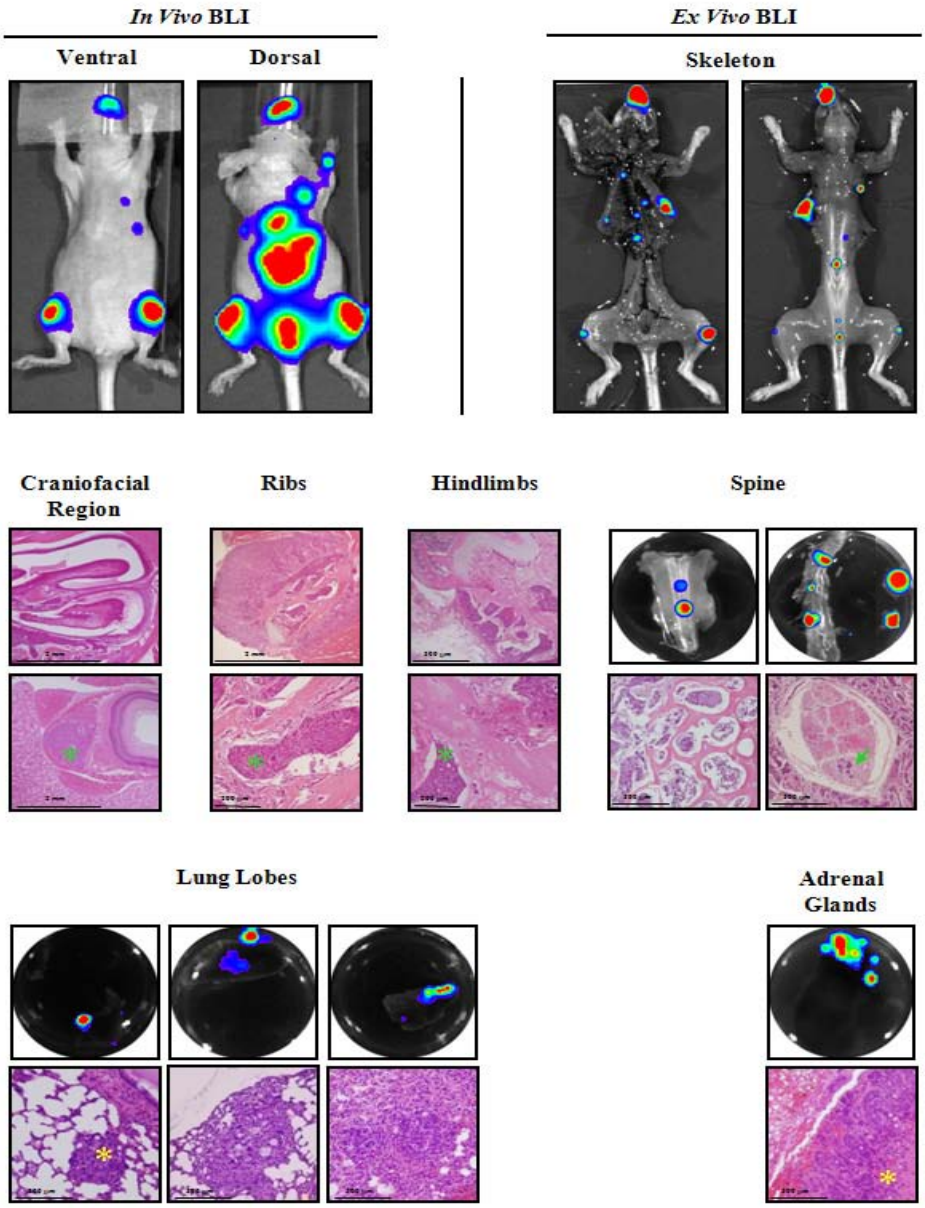

Figure 11: *Ex vivo* BLI and histological analysis of the intracardiac metastatic lesions.
Ex vivo BLI and histopathology of excised tissues confirmed the presence of bone metastatic growth into the craniofacial region (micrometastases in the ethmoturbinates of the nasal cavity, maxilla and the retrobulbar space), ribs (metastasis in the bone-marrow of ribs), hindlimbs (metastatic lesions identified in bone-marrow of distal femur, proximal tibia, periostium, and adjacent to epiphyseal growth plate) and spine (presence of metastatic cells from bone-marrow of vertebrae and its invasion to the nerve roots of *cauda equina*), and associated tissues such as lungs and adrenal glands. In terms of morphology, bone-invading cells differ from those detected in soft tissues. *Green asterisks* or *arrows* indicate bone-invading tumor cells, and *yellow asterisks* indicate soft tissue-invading tumor cells.

injection was primarily to bone sites including craniofacial region, ribs, hindlimbs and spine (Figure 11 and Table 4). While bone is the predominant metastatic site, a high frequency of micrometastases into soft tissues such as lungs and adrenal glands were also identified. Moreover, in terms of morphology, bone-invading cells differ from those detected in soft tissues. Neoplastic cells growing in bone-marrow had polygonal shape probably as an adaptation to bone microenvironment; in contrast to cells found in soft tissues that showed round to oval shape. Apart from this, and despite the poor cell differentiation, their epithelial origins were evident because in both cases cells showed the capability to form *acini*-like structures. Therefore, microenvironmental differences between bone-marrow and other tissues suggest that metastases to bone-marrow may require very different cellular characteristics than those to soft-tissues [44]. Metastases in bone are found invariably in sites adjacent to red bone-marrow, indicating that the hematopoietic marrow, rather than the bone tissue, is the initial site of cancer cell seeding [48]. This suggests that the injected tumor cells lodge, survive in the hematopoietic bone-marrow environment, and grow to destroy adjacent bone. This novel model of CRC bioluminescent bone metastases will provide

Table 4: Metastatic lesions after intracardiac injection of HT-29 CRC bioluminescent cells.

	Metastasis Incidence [Mice (%)]
Skeletal metastases:	
Craniofacial region	6/6 (100)
Ribs	6/6 (100)
Hindlimbs	4/6 (67)
Spine	4/6 (67)
Soft tissues metastases:	
Axillaryl lymph nodes	3/6 (50)
Lungs	6/6 (100)
Adrenal glands	6/6 (100)

the opportunity for exploring factors involved in tumor growth in bone, and for appropriate testing of new therapeutic strategies for life threatening bone and bone-marrow metastasis.

Conclusion

BLI allowed broadening the range of animal models to study CRC advanced disease. By means of subcutaneous models, we have demonstrated that BLI is an appropriate and reliable tool to noninvasively evaluate tumor burden and anticancer treatment efficacy. Moreover, BLI has allowed the discovery of unexpected metastatic sites for an ectopic model, such as lymphatic and hematogenous metastases. Importantly, the orthotopic implantation of tumor cells into the cecum allows the study in the proper microenviroment and provides two CRC models with different patterns of spontaneous dissemination that includes all the steps of the metastatic progression, thereby resembling the clinical setting most closely. Last, liver and bone metastasis models permit longitudinal studies of its development with high sensitivity, providing novel models to assess specific new therapeutic strategies against CRC hepatic and bone metastasis. In all animal models, the use of *in vivo* BLI has permitted the tracking over time of the CRC disease, and *ex vivo* BLI confirmed the location of *in vivo* BLI metastases and helped to identify new tissue micrometastases. Depending on the implantation site used to generate the model, the HT-29 and HCT 116 bioluminescent cells induce a different pattern and yield of metastases. Thus, the researcher can choose to use a particular cell line and implantation route to potentiate the generation of metastasis at specific sites (e.g. orthotopic for coelomic dissemination or intracardiac for skeletal metastasis). Both academic and pharmaceutical preclinical research could benefit of using the BLI technology and applications described above since they provide valuable molecular information to bridge between preclinical and early clinical studies.

Acknowledgements

This study was supported by grants from CIBER-BBN (NanoMets Intramural Grant), "Fondo de Investigaciones Sanitarias - Instituto de Salud Carlos III" (FIS-ISCIII) (PI14/02079 to SS and PS09/00965 to RM), Spanish Ministry of Science and Innovation (MICINN, IPT-090000-2010-0001 to IA), all co-funded by FEDER; and "Fundació Marató TV3" (PENTRI project 337/C/2013 to IA) and SGR (2014 SGR 1394). LS was a recipient of a pre-doctoral fellowship from FIS-ICSIII (FIS07/00002) and RH had a Miguel Servet contract (ISCIII CP13/00252).

The authors wish to thank María Dolores de la Fuente, Dr. Santiago Rojas and Dr. Juan Domingo Gispert (Institut d'Alta Tecnologia-PRBB, Barcelona, Spain) for their assistance conducting the PET studies, and Patricia Alamo (Institut de Recerca de l'Hospital de la Santa Creu i Sant Pau, Barcelona, Spain) for her help performing the orthotopic microinjections.

References

1. Siegel R, Desantis C, Jemal A. Colorectal cancer statistics, 2014. CA Cancer J Clin. 2014; 64: 104-117.
2. Torre LA, Bray F, Siegel RL, Ferlay J, Lortet-Tieulent J, Jemal A. Global cancer statistics, 2012. CA Cancer J Clin. 2015; 65: 87-108.
3. Gennatas C, Michalaki V, Gennatas S, Papalambros E. Irinotecan plus capecitabine as first-line chemotherapy in advanced colorectal cancer. Anticancer Res. 2008; 28: 1923-1926.
4. Hugen N, van de Velde CJ, de Wilt JH, Nagtegaal ID. Metastatic pattern in colorectal cancer is strongly influenced by histological subtype. Ann Oncol. 2014; 25: 651-657.
5. Kanthan R, Loewy J, Kanthan SC. Skeletal metastases in colorectal carcinomas: a Saskatchewan profile. Dis Colon Rectum. 1999; 42: 1592-1597.
6. Sundermeyer ML, Meropol NJ, Rogatko A, Wang H, Cohen SJ. Changing patterns of bone and brain metastases in patients with colorectal cancer. Clin Colorectal Cancer. 2005; 5: 108-113.
7. Wan L, Pantel K, Kang Y. Tumor metastasis: moving new biological insights into the clinic. Nat Med. 2013; 19: 1450-1464.
8. Fidler IJ. Orthotopic implantation of human colon carcinomas into nude mice provides a valuable model for the biology and therapy of metastasis. Cancer Metastasis Rev. 1991; 10: 229-243.
9. de Jong GM, Aarts F, Hendriks T, Boerman OC, Bleichrodt RP. Animal models for liver metastases of colorectal cancer: research review of preclinical studies in rodents. J Surg Res. 2009; 154: 167-176.
10. Arguello F, Baggs RB, Frantz CN. A murine model of experimental metastasis to bone and bone marrow. Cancer Res. 1988; 48: 6876-6881.
11. Griffini P, Fehres O, Klieverik L, Vogels IM, Tigchelaar W, Smorenburg SM, et al. Dietary omega-3 polyunsaturated fatty acids promote colon carcinoma metastasis in rat liver. Cancer Res. 1998; 58: 3312-3319.
12. Badr CE, Tannous BA. Bioluminescence imaging: progress and applications. Trends Biotechnol. 2011; 29: 624-633.
13. Ma X, Hui H, Shang W, Jia X, Tian J. Recent Advances in Optical Molecular Imaging and its Applications in Targeted Drug Delivery. Curr Drug Targets. 2015 Jan 1. [Epub ahead of print].
14. Cevenini L, Calabretta MM, Calabria D, Roda A, Michelini E. Luciferase Genes as Reporter Reactions: How to Use Them in Molecular Biology? Adv Biochem Eng Biotechnol. 2015 Apr 22. [Epub ahead of print].
15. Wang Y, Tseng JC, Sun Y, Beck AH, Kung AL. Noninvasive imaging of tumor burden and molecular pathways in mouse models of cancer. Cold Spring Harb Protoc. 2015; 2015: 135-144.
16. Puaux AL, Ong LC, Jin Y, Teh I, Hong M, Chow PK, et al. A comparison of imaging techniques to monitor tumor growth and cancer progression in living animals. Int J Mol Imaging. 2011; 2011: 321538.
17. Botella P, Abasolo I, Fernández Y, Muniesa C, Miranda S, Quesada M, et al. Surface-modified silica nanoparticles for tumor-targeted delivery of camptothecin and its biological evaluation. J Control Release. 2011; 156: 246-257.
18. Cabrera S, Llauradó M, Castellví J, Fernandez Y, Alameda F, Colás E, et al. Generation and characterization of orthotopic murine models for endometrial cancer. Clin Exp Metastasis. 2012; 29: 217-227.

19. Jenkins DE, Oei Y, Hornig YS, Yu SF, Dusich J, Purchio T, et al. Bioluminescent imaging (BLI) to improve and refine traditional murine models of tumor growth and metastasis. Clin Exp Metastasis. 2003; 20: 733-744.

20. Sarraf-Yazdi S, Mi J, Dewhirst MW, Clary BM. Use of in vivo bioluminescence imaging to predict hepatic tumor burden in mice. J Surg Res. 2004; 120: 249-255.

21. Tenbaum SP, Ordóñez-Morán P, Puig I, Chicote I, Arqués O, Landolfi S, et al. Î²-catenin confers resistance to PI3K and AKT inhibitors and subverts FOXO3a to promote metastasis in colon cancer. Nat Med. 2012; 18: 892-901.

22. Céspedes MV, Espina C, García-Cabezas MA, Trias M, Boluda A, Gómez del Pulgar MT, et al. Orthotopic microinjection of human colon cancer cells in nude mice induces tumor foci in all clinically relevant metastatic sites. Am J Pathol. 2007; 170: 1077-1085.

23. Scatena CD, Hepner MA, Oei YA, Dusich JM, Yu SF, Purchio T, et al. Imaging of bioluminescent LNCaP-luc-M6 tumors: a new animal model for the study of metastatic human prostate cancer. Prostate. 2004; 59: 292-303.

24. Szentirmai O, Baker CH, Lin N, Szucs S, Takahashi M, Kiryu S, Kung AL, Mulligan RC, Carter BS. Noninvasive bioluminescence imaging of luciferase expressing intracranial U87 xenografts: correlation with magnetic resonance imaging determined tumor volume and longitudinal use in assessing tumor growth and antiangiogenic treatment effect. Neurosurgery. 2006 Feb;58(2):365-72.

25. Zhang Q, Du Y, Xue Z, Chi C, Jia X, Tian J. Comprehensive evaluation of the anti-angiogenic and anti-neoplastic effects of Endostar on liver cancer through optical molecular imaging. PLoS One. 2014; 9: e85559.

26. Dickson PV, Hamner B, Ng CY, Hall MM, Zhou J, Hargrove PW, et al. *In vivo* bioluminescence imaging for early detection and monitoring of disease progression in a murine model of neuroblastoma. J Pediatr Surg. 2007; 42: 1172-1179.

27. Meuwissen R, Jonkers J, Berns A. Mouse models for sporadic cancer. Exp Cell Res. 2001; 264: 100-110.

28. Heijstek MW, Kranenburg O, Borel Rinkes IH. Mouse models of colorectal cancer and liver metastases. Dig Surg. 2005; 22: 16-25.

29. Radinsky R, Fidler IJ. Regulation of tumor cell growth at organ-specific metastases. In Vivo. 1992; 6: 325-331.

30. Takahashi Y, Ellis LM, Wilson MR, Bucana CD, Kitadai Y, Fidler IJ. Progressive upregulation of metastasis-related genes in human colon cancer cells implanted into the cecum of nude mice. Oncol Res. 1996; 8: 163-169.

31. Killion JJ, Radinsky R, Fidler IJ. Orthotopic models are necessary to predict therapy of transplantable tumors in mice. Cancer Metastasis Rev. 1998; 17: 279-284.

32. Rajput A, Dominguez San Martin I, Rose R, Beko A, Levea C, Sharratt E, et al. Characterization of HCT116 human colon cancer cells in an orthotopic model. J Surg Res. 2008; 147: 276-281.

33. Sakuma S, Yano T, Masaoka Y, Kataoka M, Hiwatari K, Tachikawa H, et al. *In vitro/in vivo* biorecognition of lectin-immobilized fluorescent nanospheres for human colorectal cancer cells. J Control Release. 2009; 134: 2-10.

34. Sakuma S, Yano T, Masaoka Y, Kataoka M, Hiwatari K, Tachikawa H, et al. Detection of early colorectal cancer imaged with peanut agglutinin-immobilized fluorescent nanospheres having surface poly(N-vinylacetamide) chains. Eur J Pharm Biopharm. 2010; 74: 451-460.

35. Wendt MK, Drury LJ, Vongsa RA, Dwinell MB. Constitutive CXCL12 expression induces anoikis in colorectal carcinoma cells. Gastroenterology. 2008; 135: 508-517.

36. Devaud C, Rousseau B, Netzer S, Pitard V, Paroissin C, Khairallah C, et al. Anti-metastatic potential of human Vdelta1(+) gammadelta T cells in an orthotopic mouse xenograft model of colon carcinoma. Cancer Immunol Immunother. 2013; 62: 1199-1210.

37. Hoffman RM. Orthotopic metastatic (MetaMouse) models for discovery and development of novel chemotherapy. Methods Mol Med. 2005; 111: 297-322.

38. Badr CE. Bioluminescence imaging: basics and practical limitations. Methods Mol Biol. 2014; 1098: 1-18.

39. Abasolo I, Pujal J, Rabanal RM, Serafin A, Navarro P, Millán O, et al. FDG PET imaging of Ela1-myc mice reveals major biological differences between pancreatic acinar and ductal tumours. Eur J Nucl Med Mol Imaging. 2009; 36: 1156-1166.

40. Gatenby RA, Gillies RJ. Why do cancers have high aerobic glycolysis? Nat Rev Cancer. 2004; 4: 891-899.

41. Cao Q, Li ZB, Chen K, Wu Z, He L, Neamati N, et al. Evaluation of biodistribution and anti-tumor effect of a dimeric RGD peptide-paclitaxel conjugate in mice with breast cancer. Eur J Nucl Med Mol Imaging. 2008; 35: 1489-1498.

42. Min JJ, Gambhir SS. Molecular imaging of PET reporter gene expression. Handb Exp Pharmacol. 2008 (185 Pt 2): 277-303.

43. Yan X, Ray P, Paulmurugan R, Tong R, Gong Y, Sathirachinda A, et al. A transgenic tri-modality reporter mouse. PLoS One. 2013; 8: e73580.

44. Wetterwald A, van der Pluijm G, Que I, Sijmons B, Buijs J, Karperien M, et al. Optical imaging of cancer metastasis to bone marrow: a mouse model of minimal residual disease. Am J Pathol. 2002; 160: 1143-1153.

45. van der Pluijm G, Que I, Sijmons B, Buijs JT, Löwik CW, Wetterwald A, et al. Interference with the microenvironmental support impairs the de novo formation of bone metastases in vivo. Cancer Res. 2005; 65: 7682-7690.

46. Thalheimer A, Korb D, Bonicke L, Wiegering A, Muhling B, Schneider M, et al. Noninvasive visualization of tumor growth in a human colorectal liver metastases xenograft model using bioluminescence *in vivo* imaging. J Surg Res. 2013; 185: 143-151.

47. Smakman N, Martens A, Kranenburg O, Borel Rinkes IH. Validation of bioluminescence imaging of colorectal liver metastases in the mouse. J Surg Res. 2004; 122: 225-230.

48. Willis R. The spread of tumors in the human body; London: Butterworth; 1973.

J Mol Biol & Mol Imaging - Volume 2 Issue 2 - 2015
ISSN : 2471-0237 | www.austinpublishinggroup.com

Citation: Fernández Y, Foradada L, García-Aranda N, Mancilla S, Suárez-López L, Céspedes MV, et al. Bioluminescent Imaging of Animal Models for Human Colorectal Cancer Tumor Growth and Metastatic Dissemination to Clinically Significant Sites. J Mol Biol & Mol Imaging. 2015;2(2): 1019.